

Drag and diffusion coefficients of a spherical particle attached to a fluid interface

Aaron Dörr and Steffen Hardt

Institute for Nano- and Microfluidics, Center of Smart Interfaces, Technische Universität Darmstadt, Alarich-Weiss-Straße 10, 64287 Darmstadt, Germany

(Received 20 February 2015)

Explicit analytical expressions for the drag and diffusion coefficients of a spherical particle attached to the interface between two immiscible fluids are constructed for the case of a small viscosity ratio between the fluid phases. The model is designed to explicitly account for the dependence on the contact angle between the two fluids and the solid surface. The Lorentz reciprocal theorem is applied in the context of a geometric perturbation approach, which is based on the deviation of the contact angle from a 90° -value. By testing the model against experimental and numerical data from the literature, good agreement is found within the entire range of contact angles below 90° . As an advantage of the method reported, the drag and diffusion coefficients can be calculated up to second order in the perturbation parameter, while it is sufficient to know the velocity and pressure fields only up to first order. Extensions to other particle shapes with known velocity and pressure fields are straightforward.

1. Introduction

The diffusive behavior of colloidal particles is drastically altered compared to diffusion in a bulk fluid when the particles are affected by the presence of an interface between two immiscible fluids. The motion of particles attached to a fluid interface occurs predominantly parallel to the interface, but may also involve temporary particle detachment, as can be concluded from experiments (Walder *et al.* 2010; Sriram *et al.* 2012). The phenomenon of two-dimensional interfacial diffusion is not yet fully understood, which is reflected in the variety of experimental results as well as related theoretical models. For example, Peng *et al.* (2009) and Chen & Tong (2008) have studied the influence of the surface concentration of diffusing particles on the diffusion coefficient. In the limit of infinite dilution, the measured diffusion coefficient is found to be very close to the bulk value in one of the fluid phases. The authors of both publications explain the data by assuming the interface as incompressible, although there is no reason to assume contamination of the interface (Peng *et al.* 2009). As another example, experimentalists have occasionally found the size dependence of the diffusion coefficient to differ from the inverse of the particle radius, a^{-1} (Du *et al.* 2012; Wang *et al.* 2011), at variance with the modified Stokes-Einstein relation (Brenner & Leal 1978)

$$D = \frac{kT}{6\pi\mu_1 a f(\Theta, \mu_2/\mu_1)}. \quad (1.1)$$

By the index 1 we denote the fluid with the higher viscosity μ_1 , while index 2 denotes the fluid having the lower viscosity. The three-phase contact angle Θ is measured in fluid 1. In equation (1.1), the function f specifies the deviation of the drag force from the Stokes drag of a spherical particle suspended in the bulk of fluid 1. In terms of the drag force \mathbf{F}_D

acting on the attached particle, f is thus defined by

$$\mathbf{F}_D = -6\pi\mu_1 a f \mathbf{U}, \quad (1.2)$$

where \mathbf{U} denotes the particle velocity relative to the undisturbed fluids. Even when the modified Stokes-Einstein relation (1.1) is valid, as we shall assume in this study, the functional form of the drag coefficient f of a translating interfacial particle is not known. A variety of theoretical and experimental studies deal with the drag coefficient of particles attached to fluid-fluid interfaces (Fulford & Blake 1986; O’Neill *et al.* 1986; Petkov *et al.* 1995; Danov *et al.* 1995, 1998; Cichocki *et al.* 2004; Fischer *et al.* 2006; Pozrikidis 2007; Ally & Amirfazli 2010; Bławzdziejewicz *et al.* 2010). However, the corresponding theoretical models mostly rely on numerical methods. With this work, we intend to contribute to the field by providing an explicit analytical expression for the drag coefficient of a spherical particle attached to a pure interface between two fluids of highly different viscosity. According to the Stokes-Einstein relation (1.1), the diffusion coefficient D directly follows from the drag coefficient f . Our analysis aims at the latter, which can be studied by means of low Reynolds number hydrodynamics. The main feature of the new model is to account for the dependence of the drag and diffusion coefficients on the three-phase contact angle.

2. Series Expansion of the Flow Field

Our modeling focuses on the drag coefficient of a rigid sphere translating along a fluid-fluid interface at low Reynolds number. We hereby study the fundamental case of a pure fluid-fluid interface. Therefore, we do not employ any incompressibility constraint for the interface and assume a vanishing interfacial viscosity. Also, we neglect any deformation of the fluid-fluid interface on the scale of the particle radius a , corresponding to a negligible influence of external forces acting normal to the fluid-fluid interface, such as buoyancy or electromagnetic forces. Assuming a planar interface also implies that the capillary number $Ca := \mu_1 U / \sigma$ (with $U = \|\mathbf{U}\|$ and the fluid-fluid interfacial tension σ), measuring dynamic deformations of the fluid-fluid interface, is small compared to unity (Radoev *et al.* 1992). In addition to interfacial deformations, we neglect particle rotation. The validity of this assumption depends on the conditions at the three-phase contact line, for which two limiting cases exist. Firstly, the contact line can be pinned to defects of the particle surface, meaning that it retains a fixed position with respect to the latter. A pinned contact line prevents the particle from rotating if the capillary forces due to the fluid-fluid interface are sufficiently large. Secondly, the contact line can move tangentially to the particle surface if the contact-angle hysteresis is small or vanishes. In this case, the particle may rotate with an angular velocity Ω dependent on the rate of dissipation occurring at the contact line. If the angular velocity is negligible compared to U/a , the particle may be approximately considered non-rotating, because then the particle’s surface velocity associated with the rotational motion is much smaller than the surface velocity U associated with the translational motion. For increasing angular velocity, that is, decreasing dissipation at the moving contact line, the assumption of a non-rotating particle loses its validity. Consequently, the following model is valid for a particle with $\Omega a / U \ll 1$. To further simplify the mathematical treatment, we assume a vanishing viscosity ratio between the two fluids, $\mu_2 / \mu_1 \rightarrow 0$. Thus the planar fluid-fluid interface effectively becomes a symmetry plane from the viewpoint of fluid 1, while the influence of fluid 2 can be neglected. For this reason, the flow problem is analogous to the motion of a body possessing reflection symmetry moving parallel to its symmetry plane. Clearly, for a contact angle Θ of 90° , the symmetric body is spherical, resulting in the

classical Stokes flow problem around a sphere. The corresponding drag on an interfacial particle is then simply half the Stokes drag in the bulk of fluid 1 (Radoev *et al.* 1992; Danov *et al.* 1995; Petkov *et al.* 1995; Ally & Amirfazli 2010), implying

$$f(90^\circ, 0) = 1/2, \quad (2.1)$$

where the function f is defined by equation (1.1). For contact angles differing from 90° , the symmetric body consists of two fused spheres (cf. figure 1(b)). This case has been studied by Zabaranin (2007), who provides drag coefficient values derived from a numerical solution of a Fredholm integral equation. Recently, Dörr & Hardt (2014) have derived the asymptotic expression

$$f(\Theta, 0) = \frac{1}{2} \left[1 + \frac{9}{16} \cos \Theta + \mathcal{O}(\cos^2 \Theta) \right]. \quad (2.2)$$

The result (2.2) has been obtained following a method by Brenner (1964) (cf. Dörr & Hardt (2014) concerning necessary corrections to the method), which is based on spherical harmonics expansions and yields the velocity and pressure fields around a slightly deformed sphere. To this end, the particle shape (given by the pair of fused spheres of radius a in our case) needs to be parameterised in spherical coordinates (r, θ, φ) according to

$$r = r_p(\theta, \varphi), \quad (2.3)$$

and subsequently expanded in a power series

$$r_p(\theta, \varphi) = a \left[1 + \varepsilon \phi^{(1)}(\theta, \varphi) + \varepsilon^2 \phi^{(2)}(\theta, \varphi) + \dots \right] \quad (2.4)$$

in terms of a small parameter ε . Here, we choose $\varepsilon = \cos \Theta$, so that $2\varepsilon a$ equals the distance between the centers of the fused spheres. Accordingly, if we assume the centers of the spheres to lie on the x -axis with the symmetry plane given by $x = 0$, the particle shape is described by

$$r_p(\theta, \varphi) = a \left[1 + \varepsilon \sin \theta |\cos \varphi| + \varepsilon^2 \frac{\sin^2 \theta \cos^2 \varphi - 1}{2} + \dots \right], \quad (2.5)$$

from which the functions $\phi^{(1)}$ and $\phi^{(2)}$ in equation (2.4) can be read off. At the same time, the velocity and pressure fields, \mathbf{u} and p , are written in the form

$$\mathbf{u} = \mathbf{u}^{(0)} + \varepsilon \mathbf{u}^{(1)} + \varepsilon^2 \mathbf{u}^{(2)} + \mathcal{O}(\varepsilon^3), \quad \text{and} \quad (2.6)$$

$$p = p^{(0)} + \varepsilon p^{(1)} + \varepsilon^2 p^{(2)} + \mathcal{O}(\varepsilon^3). \quad (2.7)$$

The particle moves with the velocity $\mathbf{U} = U \mathbf{e}_z$. Therefore, the flow field obeys the boundary conditions

$$\mathbf{u}|_{\Sigma_p} = \mathbf{U} \quad (2.8)$$

at the particle surface Σ_p , and

$$\mathbf{u}|_{\Sigma_\infty} = 0 \quad (2.9)$$

on a spherical surface Σ_∞ at $r \rightarrow \infty$. While condition (2.9) is readily adapted to the perturbation expansion (2.6), condition (2.8) on the particle surface requires a Taylor series expansion for removal of the implicit dependence on the shape parameter ε . To be precise, the boundary condition (2.8) in conjunction with the expanded particle shape (2.4) reads

$$\mathbf{u}(r_p, \theta, \varphi) = \mathbf{U}, \quad (2.10)$$

which equals

$$\mathbf{u}^{(0)}(r_p, \theta, \varphi) + \varepsilon \mathbf{u}^{(1)}(r_p, \theta, \varphi) + \varepsilon^2 \mathbf{u}^{(2)}(r_p, \theta, \varphi) + \mathcal{O}(\varepsilon^3) = \mathbf{U}. \quad (2.11)$$

In equation (2.11), the argument r_p depends on ε , so that the velocity vectors $\mathbf{u}^{(i)}$ ($i \in \{0, 1, 2\}$) are to be expanded in a Taylor series about $r = a$ in powers of ε , using equation (2.4). After performing the expansions, inserting the results into equation (2.11), and grouping of terms, we arrive at

$$\left. \begin{aligned} \mathbf{u}^{(0)} &= \mathbf{U} \\ \mathbf{u}^{(1)} &= -a\phi^{(1)} \frac{\partial \mathbf{u}^{(0)}}{\partial r} \\ \mathbf{u}^{(2)} &= -a\phi^{(2)} \frac{\partial \mathbf{u}^{(0)}}{\partial r} - \frac{a^2}{2} [\phi^{(1)}]^2 \frac{\partial^2 \mathbf{u}^{(0)}}{\partial r^2} - a\phi^{(1)} \frac{\partial \mathbf{u}^{(1)}}{\partial r} \end{aligned} \right\} \text{at } r = a. \quad (2.12)$$

Clearly, the zeroth order problem corresponds to a spherical particle moving with constant velocity \mathbf{U} in an unbounded fluid, for which the velocity and pressure fields

$$\mathbf{u}^{(0)} = -\frac{1}{2}U \left(\frac{a}{r}\right)^2 \left(\frac{a}{r} - 3\frac{r}{a}\right) \cos\theta \mathbf{e}_r - \frac{1}{4}U \left(\frac{a}{r}\right)^2 \left(\frac{a}{r} + 3\frac{r}{a}\right) \sin\theta \mathbf{e}_\theta, \text{ and} \quad (2.13)$$

$$p^{(0)} = \frac{3}{2}\mu_1 U a \frac{\cos\theta}{r^2} \quad (2.14)$$

are well known (Happel & Brenner 1983). The first-order problem has been solved by Dörr & Hardt (2014) in the particle's rest frame. Because the frame of reference only affects the zeroth-order flow $\mathbf{u}^{(0)}$ by addition or subtraction of the velocity field $U\mathbf{e}_z$, the first-order flow field $\mathbf{u}^{(1)}$ considered by Dörr & Hardt (2014) may be directly used in the present study. The supplementary material contains the complete set of expressions required to calculate the velocity field $\mathbf{u}^{(1)}$. Since $\mathbf{u}^{(1)}$ is equal to the infinite series $\sum_{k=0}^{\infty} \mathbf{u}_k^{(1)}$ (Brenner 1964), the number of included terms needs to be limited in practical calculations. The values reported below as well as in the supplementary information correspond to $k \leq 20$. With this choice, the $\mathcal{O}(\varepsilon^2)$ -contribution to the drag coefficient can be calculated to three significant digits, as will be shown in the following section.

3. Applying the Lorentz Reciprocity Theorem

According to the above discussion, we are in a position to compute the velocity fields $\mathbf{u}^{(i)}(a, \theta, \varphi)$, $i \in \{0, 1, 2\}$, on a spherical surface by means of equation (2.12). In other words, we are faced with two flow problems involving a sphere of radius a in an unbounded fluid, see figure 1. The first of these problems (figure 1(a)), constructed by setting ε to zero, consists of a sphere with a no-slip surface condition and translating with velocity $U\mathbf{e}_z$. We shall denote the velocity and stress tensor fields belonging to this first problem by $\hat{\mathbf{u}}$ and $\hat{\boldsymbol{\tau}}$, respectively. The second problem (figure 1(b)), associated with the truncated perturbation expansion in ε and denoted by \mathbf{u} and $\boldsymbol{\tau}$, is given by a sphere with a prescribed surface velocity field of

$$\mathbf{u}(a, \theta, \varphi) = \sum_{i=0}^{\infty} \varepsilon^i \mathbf{u}^{(i)}(a, \theta, \varphi) = U\mathbf{e}_z + \varepsilon \mathbf{u}^{(1)}(a, \theta, \varphi) + \varepsilon^2 \mathbf{u}^{(2)}(a, \theta, \varphi) + \mathcal{O}(\varepsilon^3), \quad (3.1)$$

according to equation (2.12). Since the solutions $(\hat{\mathbf{u}}, \hat{\boldsymbol{\tau}})$ and $(\mathbf{u}, \boldsymbol{\tau})$ correspond to the same flow geometry, they are related by the Lorentz reciprocal theorem for Stokes flow (Lorentz

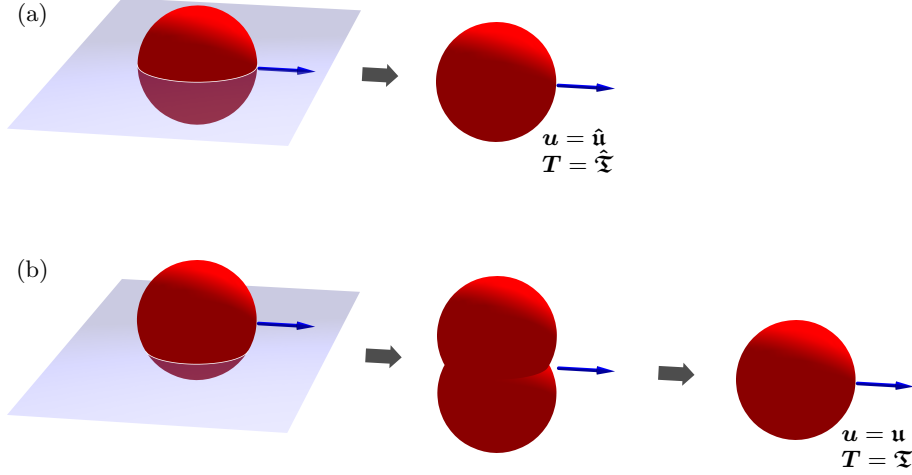


FIGURE 1. Pair of flow problems connected by the Lorentz reciprocal theorem (3.2): (a) a sphere moving along a fluid-fluid interface with vanishing viscosity ratio causes a flow field identical to the classical Stokes flow problem in a bulk fluid, denoted by $\hat{\mathbf{u}}$ and $\hat{\mathbf{T}}$, if the contact angle Θ equals 90° ; (b) for $\Theta \neq 90^\circ$, the flow problem is equivalent to a pair of fused spheres moving through a bulk fluid; by means of a perturbation expansion, the boundary condition on the complex particle surface is projected onto a sphere; the flow field in this case is denoted by \mathbf{u} and \mathbf{T} .

1896; Happel & Brenner 1983),

$$\int_{\Sigma} (\hat{\mathbf{T}} \cdot \mathbf{n}) \cdot \mathbf{u} \, d\Sigma = \int_{\Sigma} (\mathbf{T} \cdot \mathbf{n}) \cdot \hat{\mathbf{u}} \, d\Sigma, \quad (3.2)$$

where Σ comprises the particle surface Σ_p (outer normal vector $\mathbf{n} = -\mathbf{e}_r$) and the surface Σ_∞ at infinity (outer normal vector $\mathbf{n} = \mathbf{e}_r$). The Lorentz theorem (3.2) has been exploited in a number of cases, for instance by Stone & Samuel (1996), Masoud & Stone (2014), and Schönecker & Hardt (2014). Its use in the present study is inspired by the argumentation of Stone & Samuel (1996). The contribution from the integral over Σ_∞ in equation (3.2) vanishes because

$$\|\hat{\mathbf{u}}\| \sim r^{-1}, \quad \|\mathbf{u}\| \sim r^{-1}, \quad \|\hat{\mathbf{T}} \cdot \mathbf{e}_r\| \sim r^{-2}, \quad \text{and} \quad \|\mathbf{T} \cdot \mathbf{e}_r\| \sim r^{-2} \quad \text{for } r \rightarrow \infty. \quad (3.3)$$

The integral in the Lorentz theorem (3.2) thus reduces to an integral over the particle surface Σ_p . Recalling that $\hat{\mathbf{T}} \cdot \mathbf{n} = -\hat{\mathbf{T}} \cdot \mathbf{e}_r = 3\mu_1 U / (2a) \mathbf{e}_z$ (Stone & Samuel 1996) and using equation (3.1), the Lorentz theorem can be written as

$$\int_{\Sigma_p} \frac{3\mu_1}{2a} U \mathbf{e}_z \cdot \left[U \mathbf{e}_z + \varepsilon \mathbf{u}^{(1)} + \varepsilon^2 \mathbf{u}^{(2)} + \mathcal{O}(\varepsilon^3) \right] d\Sigma = \int_{\Sigma_p} (\mathbf{T} \cdot \mathbf{n}) \cdot U \mathbf{e}_z d\Sigma. \quad (3.4)$$

Since $U \mathbf{e}_z$ is a constant vector and $\int_{\Sigma_p} d\Sigma = 4\pi a^2$, equation (3.4) simplifies to

$$6\pi\mu_1 U + \frac{3\mu_1}{2a} \mathbf{e}_z \cdot \int_{\Sigma_p} \left[\varepsilon \mathbf{u}^{(1)} + \varepsilon^2 \mathbf{u}^{(2)} + \mathcal{O}(\varepsilon^3) \right] d\Sigma = \mathbf{e}_z \cdot \underbrace{\int_{\Sigma_p} \mathbf{T} \cdot \mathbf{n} d\Sigma}_{=-\mathbf{F}_D}. \quad (3.5)$$

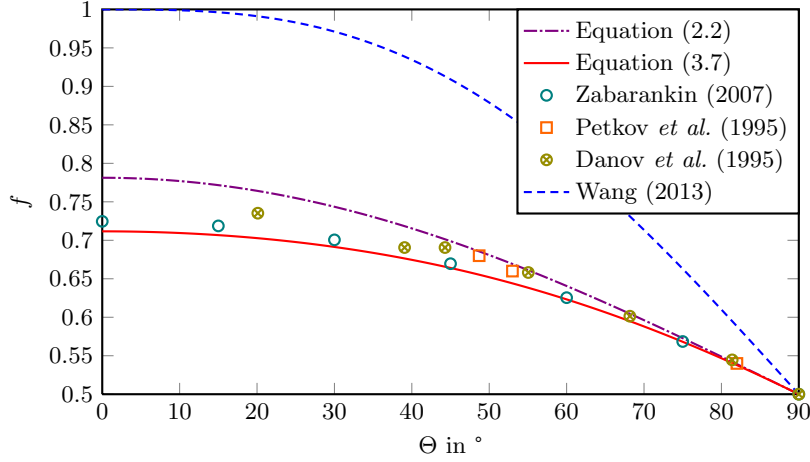


FIGURE 2. Comparison of the models (2.2) and (3.7) with experimental and theoretical drag coefficient values taken from the literature. In the experiments by Petkov *et al.* (1995), an air-water interface with a very small viscosity ratio, $\mu_2/\mu_1 \approx 0.02$, was studied. The remaining curves are valid under the assumption $\mu_2/\mu_1 = 0$.

The integral on the right-hand-side of equation (3.5) has been identified with the negative of the Stokes drag \mathbf{F}_D on the particle because $\mathbf{n} = -\mathbf{e}_r$. Using equations (2.12), (2.13), (2.4), and (2.5) in conjunction with the velocity field $\mathbf{u}^{(1)}$ according to Dörr & Hardt (2014), the integral occurring in equation (3.5) can be evaluated, yielding

$$\mathbf{F}_D \cdot \mathbf{e}_z = -6\pi\mu_1 Ua \left[1 + \frac{9}{16}\varepsilon - 0.139\varepsilon^2 + \mathcal{O}(\varepsilon^3) \right]. \quad (3.6)$$

From the symmetry of the problem, it clearly follows that $\mathbf{F}_D = F_D \mathbf{e}_z$, so that the drag coefficient (1.2) for the original problem of a spherical particle diffusing along a fluid-fluid interface of zero viscosity ratio is given by

$$f(\Theta, 0) = \frac{1}{2} \left[1 + \frac{9}{16} \cos \Theta - 0.139 \cos^2 \Theta + \mathcal{O}(\cos^3 \Theta) \right]. \quad (3.7)$$

Correspondingly, for the diffusion coefficient (1.1) it follows that

$$D = \frac{16kT}{3\pi\mu_1 a [16 + 9 \cos \Theta + 2.224 \cos^2 \Theta + \mathcal{O}(\cos^3 \Theta)]}. \quad (3.8)$$

Note that the numerical coefficient 0.139 in equation (3.7) can be calculated to any desired number of significant digits, provided that a sufficient number of terms is considered in the spherical harmonics expansion by Brenner (1964) and Dörr & Hardt (2014). As stated above, the value 0.139... corresponds to a number of 20 terms. The underlying rational expression reads $765\,368\,413\,099/5\,497\,558\,138\,880$.

4. Discussion

In figure 2, we compare the result (3.7) and its first-order part (2.2) to experimental and theoretical drag coefficient values from the literature. The numerical solution to the full flow problem by Zabaranin (2007) may serve as a reference. Remarkably, equation (2.2) can be seen to be applicable at least down to a contact angle of 60° , where it still agrees well with the reference data. The inclusion of the $\cos^2 \Theta$ -term, resulting in equation (3.7),

leads to a significantly better agreement between the asymptotic model and the numerical solution. Within a maximum error in the drag coefficient f of less than 0.02 (3%), the quadratic expression may even be applied to the full range of contact angles between 0 and 90°. An approximate formula by Wang (2013),

$$f_W = 1 + \frac{\sin(2\Theta) - 2\Theta}{2\pi}, \quad (4.1)$$

based on the particle's cross-sectional area seen by the respective fluid phases is also plotted in figure 2. Apparently, this expression is at variance with the other four data sets shown in the figure. The region where $\Theta > 90^\circ$ is excluded from figure 2 owing to a lack of reference data. The drag coefficient is expected to approach zero when the contact angle approaches 180°, a behaviour which is not reproduced by the model equation (3.7). Therefore, the range of validity of the model for contact angles larger than 90° remains an open issue. In order to model the drag coefficient near 180°, either the above perturbation expansion would need to be extended to higher orders in ε , or a reference body differing from a sphere (such as a disk or an ellipsoid) would need to be used.

5. Conclusions

With equations (3.7) and (3.8), we have developed explicit expressions for the drag and diffusion coefficients of a spherical particle attached to the interface between two immiscible fluids for the case of a small viscosity ratio between the two phases. The relations account for the dependence on the contact angle between the two fluids and the solid surface. Following from the assumption on the viscosity ratio, the drag and diffusion coefficients of a pair of fused spheres moving perpendicular to their line-of-centers has been found simultaneously. A comparison between the model and reference data has shown that the model can be applied to the entire range of contact angles below 90° with high accuracy. By applying the Lorentz reciprocal theorem to a geometric perturbation expansion, one order of approximation has been gained for the drag and diffusion coefficients as compared to the flow field. In other words, the second-order result (3.7) is based on the first-order velocity field, while calculating the non-trivial first-order result (2.2) only requires the well-known flow field around a sphere. The method can be applied to any particle shape resulting from a small geometric modification of another particle shape with a known flow field.

Acknowledgments

We gratefully acknowledge financial support by the German Research Foundation through Grant No. HA 2696/25-1.

REFERENCES

- ALLY, J. & AMIRFAZLI, A. 2010 Magnetophoretic measurement of the drag force on partially immersed microparticles at air-liquid interfaces. *Colloids and Surfaces A: Physicochem. Eng. Aspects* **360**, 120–128.
- BŁAWZDZIEWICZ, J., EKIEL-JEŻEWSKA, M.L. & WAJNRYB, E. 2010 Motion of a spherical particle near a planar fluid-fluid interface: The effect of surface incompressibility. *J. Chem. Phys.* **133**, 114702.
- BRENNER, H. 1964 The Stokes resistance of a slightly deformed sphere. *Chem. Eng. Sci.* **19**, 519–539.
- BRENNER, H. & LEAL, L.G. 1978 A micromechanical derivation of Fick's law for interfacial diffusion of surfactant molecules. *J. Colloid Interface Sci.* **65** (2), 191–209.

- CHEN, W. & TONG, P. 2008 Short-time self-diffusion of weakly charged silica spheres at aqueous interfaces. *Eur. Phys. Lett.* **84**, 28003.
- CICHOCKI, B., EKIEL-JEEWSKA, M.L., NÄGELE, G. & WAJNRYB, E. 2004 Motion of spheres along a fluid-gas interface. *J. Chem. Phys.* **121**, 2305.
- DANOV, K., AUST, R., DURST, F. & LANGE, U. 1995 Influence of the surface viscosity on the hydrodynamic resistance and surface diffusivity of a large Brownian particle. *J. Colloid Interface Sci.* **175**, 36–45.
- DANOV, K.D., GURKOV, T.D., RASZILLIER, H. & DURST, F. 1998 Stokes flow caused by the motion of a rigid sphere close to a viscous interface. *Chem. Eng. Sci.* **53** (19), 3413–3434.
- DÖRR, A. & HARDT, S. 2014 Driven particles at fluid interfaces acting as capillary dipoles. arXiv:1411.1183v1 [cond-mat.soft].
- DU, K., LIDDLE, J.A. & BERGLUND, A.J. 2012 Three-dimensional real-time tracking of nanoparticles at an oil-water interface. *Langmuir* **28**, 9181–9188.
- FISCHER, T.M., DHAR, P. & HEINIG, P. 2006 The viscous drag of spheres and filaments moving in membranes or monolayers. *J. Fluid Mech.* **558**, 451–475.
- FULFORD, G.R. & BLAKE, J.R. 1986 Force distribution along a slender body straddling an interface. *J. Austral. Math. Soc. Ser. B* **27**, 295–315.
- HAPPEL, J. & BRENNER, H. 1983 *Low Reynolds number hydrodynamics*. The Hague: Martinus Nijhoff Publishers.
- LORENTZ, H.A. 1896 Eene algemeene stelling omtrent de beweging eerier vloeistof met wrijving en eenige daarmit afgeleide gevolgen. *Zittingsverslag van de Koninklijke Akademie van Wetenschappen te Amsterdam* **5**, 168–175, translation into English: *Journal of Engineering Mathematics* **30**: 19–24, 1996.
- MASOUD, H. & STONE, H.A. 2014 A reciprocal theorem for marangoni propulsion. *J. Fluid Mech.* **741** R4, 1–7.
- O’NEILL, M.E., RANGER, K.B. & BRENNER, H. 1986 Slip at the surface of a translating-rotating sphere bisected by a free surface bounding a semiinfinite viscous fluid: Removal of the contactline singularity. *Phys. Fluids* **29**, 913.
- PENG, Y., CHEN, W., FISCHER, TH.M., WEITZ, D.A. & TONG, P. 2009 Short-time self-diffusion of nearly hard spheres at an oil-water interface. *J. Fluid Mech.* **618**, 243–261.
- PETKOV, J.T., DENKOV, N.D., DANOV, K.D., VELEV, O.D., AUST, R. & DURST, F. 1995 Measurement of the drag coefficient of spherical particles attached to fluid interfaces. *J. Colloid Interface Sci.* **172**, 147–154.
- POZRIKIDIS, C. 2007 Particle motion near and inside an interface. *J. Fluid Mech.* **575**, 333–357.
- RADOEV, B., NEDJALKOV, M. & DJAKOVICH, V. 1992 Brownian motion at liquid-gas interfaces. 1. Diffusion coefficients of macroparticles at pure interfaces. *Langmuir* **8**, 2962–2965.
- SCHÖNECKER, C. & HARDT, S. 2014 Electro-osmotic flow along superhydrophobic surfaces with embedded electrodes. *Phys. Rev. E* **89**, 063005.
- SRIRAM, I., WALDER, R. & SCHWARTZ, D.K. 2012 Stokes-Einstein and desorption-mediated diffusion of protein molecules at the oil-water interface. *Soft Matter* **8**, 6000.
- STONE, H.A. & SAMUEL, A.D.T. 1996 Propulsion of microorganisms by surface distortions. *Phys. Rev. Lett.* **77** (19), 4102–4104.
- WALDER, R.B., HONCIUC, A. & SCHWARTZ, D.K. 2010 Phospholipid diffusion at the oil-water interface. *J. Phys. Chem. B* **114**, 11484–11488.
- WANG, D. 2013 Tracer diffusion at water-oil interfaces studied by fluorescence correlation spectroscopy. PhD thesis, Universitätsbibliothek Mainz.
- WANG, D., YORDANOV, S., PAROOR, H.M., MUKHOPADHYAY, A., LI, C.Y., BUTT, H.-J. & KOYNOV, K. 2011 Probing diffusion of single nanoparticles at water-oil interfaces. *small* **7** (24), 3502–3507.
- ZABARANKIN, M. 2007 Asymmetric three-dimensional Stokes flow about two fused equal spheres. *Proc. R. Soc. A* **463**, 2329–2349.

Appendix A. First-order velocity field

A.1. Series representation of the velocity field

The first-order velocity field $\mathbf{u}^{(1)}$ can be calculated according to the method by Brenner (1964). However, as pointed out by Dörr & Hardt (2014), corrections to Brenner's method are necessary. Here, we provide all of the expressions required to explicitly compute the velocity field $\mathbf{u}^{(1)}$, which is of the form (Brenner 1964)

$$\mathbf{u}^{(1)} = \sum_{k=0}^{\infty} \mathbf{u}_k^{(1)}. \quad (\text{A } 1)$$

To facilitate the explicit evaluation of the velocity field and to simultaneously ensure a high degree of accuracy, we truncate the series after 20 summation terms and arrive at

$$\mathbf{u}^{(1)} \approx \sum_{k=0}^{20} \mathbf{u}_k^{(1)}. \quad (\text{A } 2)$$

The velocity fields $\mathbf{u}_k^{(1)}$ can be expressed by

$$\begin{aligned} \mathbf{u}_k^{(1)} = \sum_{n=1}^{\infty} \left[\nabla \times \left(\mathbf{r}_k \chi_{-n-1}^{(1)} \right) + \nabla \left({}_k\phi_{-n-1}^{(1)} \right) - \frac{n-2}{2n(2n-1)\mu_1} r^2 \nabla \left({}_k p_{-n-1}^{(1)} \right) \right. \\ \left. + \mathbf{r} \frac{n+1}{n(2n-1)\mu_1} {}_k p_{-n-1}^{(1)} \right], \end{aligned} \quad (\text{A } 3)$$

where

$${}_k p_{-n-1}^{(1)} = \frac{(2n-1)\mu_1}{(n+1)a} \left(\frac{a}{r} \right)^{n+1} \left[(n+2) {}_k X_n^{(1)} + {}_k Y_n^{(1)} \right], \quad (\text{A } 4)$$

$${}_k \phi_{-n-1}^{(1)} = \frac{a}{2(n+1)} \left(\frac{a}{r} \right)^{n+1} \left(n {}_k X_n^{(1)} + {}_k Y_n^{(1)} \right), \text{ and} \quad (\text{A } 5)$$

$${}_k \chi_{-n-1}^{(1)} = \frac{1}{n(n+1)} \left(\frac{a}{r} \right)^{n+1} {}_k Z_n^{(1)} \quad (\text{A } 6)$$

(Brenner 1964). Through accommodating the velocity field (A 3) to the boundary condition at the particle surface, the functions ${}_k X_n^{(1)}$, ${}_k Y_n^{(1)}$ and ${}_k Z_n^{(1)}$ can be specified. One has

$${}_k X_n^{(1)} = 0 \quad \text{for } n \leq 1, \quad (\text{A } 7)$$

$${}_k Y_n^{(1)} = \begin{cases} \frac{3}{2} \sum_{m=0}^k \frac{c_{km} N_{km} \cos(m\varphi)}{2k+1} (k-1)(k+m) P_{k-1}^m(\cos\theta) & \text{for } n = k-1 \\ -\frac{3}{2} \sum_{m=0}^k \frac{c_{km} N_{km} \cos(m\varphi)}{2k+1} (2+k)(k-m+1) P_{k+1}^m(\cos\theta) & \text{for } n = k+1 \\ 0 & \text{for all other } n, \end{cases} \quad (\text{A } 8)$$

and

$${}_k Z_n^{(1)} = \begin{cases} \frac{3}{2} U \sum_{m=0}^k m c_{km} N_{km} P_k^m(\cos\theta) \sin(m\varphi) & \text{for } n = k \\ 0 & \text{for } n \neq k. \end{cases} \quad (\text{A } 9)$$

In equations (A 7)–(A 9), the P_k^m are associated Legendre polynomials. Expression (A 8), developed by Dörr & Hardt (2014), differs from the corresponding result by Brenner

(1964), while equations (A 7) and (A 9) have been adopted from Brenner (1964) without modification. The expansion coefficients c_{km} and N_{km} are given by

$$N_{km} = \begin{cases} \sqrt{2} \sqrt{\frac{2k+1}{4\pi}} \frac{(k-m)!}{(k+m)!} & \text{if } m > 0 \\ \sqrt{\frac{2k+1}{4\pi}} & \text{if } m = 0 \end{cases} \quad (\text{A } 10)$$

and

$$c_{km} = \int_0^\pi \int_0^{2\pi} \sin \theta |\cos \varphi| N_{km} P_k^m(\cos \theta) \cos(m\varphi) \sin \theta d\theta d\varphi, \quad (\text{A } 11)$$

respectively. Equation (A 11) contains information about the particle geometry via the term $\sin \theta |\cos \varphi|$, which is equal to the first-order term $\phi^{(1)}$ in the expansion of the particle shape (equation (2.5) in the paper). The velocity field $\mathbf{u}^{(1)}$ according to equation (A 1) is thus fully determined. For the sake of convenience, we explicitly display the coefficients c_{km} for $k \leq 20$ in appendix A.2. Due to the symmetry of the particle shape with respect to the plane $x = 0$, coefficients with $m < 0$ and/or m odd vanish.

A.2. Coefficients c_{km}

$k=0: m=0$

$$\sqrt{\pi}$$

$k=2: m=0,2$

$$-\frac{\sqrt{5\pi}}{8}, \frac{\sqrt{15\pi}}{8}$$

$k=4: m=0,2,4$

$$-\frac{3\sqrt{\pi}}{64}, \frac{\sqrt{5\pi}}{32}, -\frac{\sqrt{35\pi}}{64}$$

$k=6: m=0,2,4,6$

$$-\frac{5\sqrt{13\pi}}{1024}, \frac{\sqrt{\frac{1365\pi}{2}}}{1024}, -\frac{3\sqrt{91\pi}}{1024}, \frac{\sqrt{\frac{3003\pi}{2}}}{1024}$$

$k=8: m=0,2,4,6,8$

$$-\frac{35\sqrt{17\pi}}{16384}, \frac{3\sqrt{\frac{595\pi}{2}}}{4096}, -\frac{3\sqrt{1309\pi}}{8192}, \frac{\sqrt{\frac{7293\pi}{2}}}{4096}, -\frac{3\sqrt{12155\pi}}{16384}$$

$k=10: m=0,2,\dots,10$

$$-\frac{147\sqrt{21\pi}}{131072}, \frac{49\sqrt{385\pi}}{131072}, -\frac{7\sqrt{5005\pi}}{65536}, \frac{21\sqrt{\frac{5005\pi}{2}}}{131072}, -\frac{7\sqrt{\frac{85085\pi}{3}}}{131072}, \frac{7\sqrt{\frac{323323\pi}{6}}}{131072}$$

$k=12: m=0,2,\dots,12$

$$-\frac{3465\sqrt{\pi}}{1048576}, \frac{45\sqrt{3003\pi}}{524288}, -\frac{225\sqrt{\frac{1001\pi}{2}}}{1048576}, \frac{75\sqrt{\frac{2431\pi}{2}}}{524288}, -\frac{15\sqrt{138567\pi}}{1048576}, \frac{15\sqrt{\frac{88179\pi}{2}}}{524288}, -\frac{15\sqrt{\frac{676039\pi}{2}}}{1048576}$$

$k=14: m=0,2,\dots,14$

$$-\frac{14157\sqrt{29\pi}}{33554432}, \frac{1089\sqrt{39585\pi}}{67108864}, -\frac{99\sqrt{\frac{2467465\pi}{2}}}{33554432}, \frac{33\sqrt{46881835\pi}}{67108864}, -\frac{33\sqrt{12785955\pi}}{33554432}, \frac{33\sqrt{58815393\pi}}{67108864},$$

$$-\frac{165\sqrt{\frac{1508087\pi}{2}}}{33554432}, \frac{495\sqrt{646323\pi}}{67108864}$$

$k=16: m=0,2,\dots,16$

$$-\frac{306735\sqrt{33\pi}}{1073741824}, \frac{20449\sqrt{935\pi}}{268435456}, -\frac{1573\sqrt{\frac{323323\pi}{2}}}{268435456}, \frac{3003\sqrt{46189\pi}}{268435456},$$

$$-\frac{1001\sqrt{\frac{5311735\pi}{3}}}{536870912}, \frac{715\sqrt{\frac{2860165\pi}{3}}}{268435456}, -\frac{2145\sqrt{\frac{245157\pi}{2}}}{268435456}, \frac{143\sqrt{35547765\pi}}{268435456}, -\frac{143\sqrt{1101980715\pi}}{1073741824}$$

$k=18: m=0,2,\dots,18$

$$-\frac{1738165\sqrt{37\pi}}{8589934592}, \frac{61347\sqrt{59755\pi}}{8589934592}, -\frac{5577\sqrt{\frac{920227\pi}{2}}}{2147483648}, \frac{1001\sqrt{\frac{117920517\pi}{2}}}{4294967296}, -\frac{15015\sqrt{274873\pi}}{4294967296},$$

$$\frac{2145\sqrt{\frac{28861665\pi}{2}}}{4294967296}, -\frac{2145\sqrt{\frac{7971317\pi}{2}}}{2147483648}, \frac{429\sqrt{\frac{3706662405\pi}{2}}}{8589934592}, -\frac{429\sqrt{2398428615\pi}}{8589934592}, \frac{715\sqrt{\frac{3357800061\pi}{2}}}{8589934592}$$

$k=20: m=0,2,\dots,20$

$$-\frac{10207769\sqrt{41\pi}}{68719476736}, \frac{48841\sqrt{899745\pi}}{34359738368}, -\frac{8619\sqrt{117266765\pi}}{68719476736}, \frac{1105\sqrt{\frac{914680767\pi}{2}}}{17179869184}, -\frac{9945\sqrt{23453353\pi}}{34359738368},$$

$$\frac{1989\sqrt{\frac{309157835\pi}{2}}}{17179869184}, -\frac{3315\sqrt{\frac{1916778577\pi}{2}}}{68719476736}, \frac{3315\sqrt{\frac{531543639\pi}{2}}}{34359738368}, -\frac{3315\sqrt{1240268491\pi}}{68719476736}, \frac{1105\sqrt{\frac{7245779079\pi}{2}}}{34359738368},$$

$$-\frac{663\sqrt{\frac{156991880045\pi}{2}}}{68719476736}$$